

Review

# A Mini-Review on Metal Oxide Semiconductor Gas Sensors for Carbon Monoxide Detection at Room Temperature

Yaoyi He<sup>1,2</sup> and Mingzhi Jiao<sup>1,2,3,\*</sup> <sup>1</sup> Tiandi (Changzhou) Automation Co., Ltd., Changzhou 213000, China<sup>2</sup> CCTEG Changzhou Research Institute, Changzhou 213000, China<sup>3</sup> National and Local Joint Engineering Laboratory of Internet Application Technology on Mine, China University of Mining and Technology, Xuzhou 221116, China

\* Correspondence: mingzhijiao@cumt.edu.cn; Tel.: +86-13952204541

**Abstract:** Carbon monoxide can cause severe harm to humans even at low concentrations. Metal Oxide Semiconductor (MOS) carbon monoxide gas sensors have excellent sensing performance regarding sensitivity, selectivity, response speed, and stability, making them very desirable candidates for carbon monoxide monitoring. However, MOS gas sensors generally work at temperatures higher than room temperature, and need a heating source that causes high power consumption. High power consumption is a great problem for long-term portable monitoring devices for point-of-care or wireless sensor nodes for IoT application. Room-temperature MOS carbon monoxide gas sensors can function well without a heater, making them rather suitable for IoT or portable applications. This review first introduces the primary working mechanism of MOS carbon monoxide sensors and then gives a detailed introduction to and analysis of room-temperature MOS carbon monoxide sensing materials, such as ZnO, SnO<sub>2</sub>, and TiO<sub>2</sub>. Lastly, several mechanisms for room-temperature carbon monoxide sensors based on MOSs are discussed. The review will be interesting to engineers and researchers working on MOS gas sensors.

**Keywords:** carbon monoxide; Metal Oxide Semiconductor; sensing mechanism; noble metals; gas sensors; room temperature



**Citation:** He, Y.; Jiao, M. A Mini-Review on Metal Oxide Semiconductor Gas Sensors for Carbon Monoxide Detection at Room Temperature. *Chemosensors* **2024**, *12*, 55. <https://doi.org/10.3390/chemosensors12040055>

Academic Editor: Boris Lakard

Received: 21 February 2024

Revised: 18 March 2024

Accepted: 20 March 2024

Published: 6 April 2024



**Copyright:** © 2024 by the authors. Licensee MDPI, Basel, Switzerland. This article is an open access article distributed under the terms and conditions of the Creative Commons Attribution (CC BY) license (<https://creativecommons.org/licenses/by/4.0/>).

## 1. Introduction

Carbon monoxide (CO) can cause headaches, discomfort, and the possibility of collapse when humans are exposed to it for two hours at a concentration of 200 ppm. At 3000 ppm, CO will cause human death after exposure for 20 min [1–5]. Thus, convenient and precise monitoring of CO is crucial for safety reasons. Electrochemical sensors, infrared sensors, and semiconductor sensors are several common sensors for measuring CO concentration. Electrochemical CO sensors have a short lifetime and high cost. Infrared CO sensors have a large volume and high price. Compared with their counterpart like an electrochemical CO sensor, semiconductor CO sensors have several advantages such as low cost, high robustness, and a long lifetime, thus are widely applied in CO monitoring [6–22]. Many semiconductors such as carbon nanotubes, metal oxides, and organic compounds have been studied for use in CO sensors [23–26]. Among all the semiconductor sensing materials, metal oxides are the cheapest and most stable ones [6–22]. It is a trend to incorporate MOS CO sensors into mobile phones or other portable devices to facilitate CO measurement [27]. MOS CO sensors employ metal oxides like SnO<sub>2</sub> as sensing elements. SnO<sub>2</sub> CO sensors usually work at temperatures higher than room temperature, so a heater is necessary to provide the optimum working temperature. The heater will consume great amounts of electrical power, increasing the overall power consumption of the CO sensors. High power consumption gives rise to a problem for portable and IoT applications of MOS CO sensors, since a large lithium battery will be needed for the power supply.

Room-temperature MOS CO gas sensors are promising for IoT applications due to the removal of the heater and reduction in power consumption. Recent years have witnessed many findings regarding MOS room-temperature CO sensing. SnO<sub>2</sub>, ZnO, and TiO<sub>2</sub> composites, especially with tailored nanostructures and doping elements, can respond to CO with high sensitivity and selectivity at room temperature. No specific review on room-temperature MOS CO sensors has been published yet, although some reviews on CO sensors above room temperature can be found [28]. This review will introduce the basic concept of sensor parameters and the sensing model first. Then, the performance and sensing mechanisms of different MOS materials are presented. A discussion of the sensing mechanisms is given after the materials section. Lastly, the conclusion with future perspectives is provided. Advances in room-temperature CO sensors will promote the application of flexible sensors since these typically need to work at room temperature on flexible substrates. Flexible sensors will be very useful in healthcare, environmental monitoring, and industrial safety [29].

## 2. General Definition and Sensing Model

The most critical parameters of MOS CO sensors are sensitivity, selectivity, response time, and recovery time [30]. The value of response/sensitivity is larger than 1. It is defined as  $R_{\text{air}}/R_{\text{gas}}$  or  $R_{\text{gas}}/R_{\text{air}}$ , where  $R_{\text{air}}$  is the resistance of the sensor in pure air, and  $R_{\text{gas}}$  refers to the resistance of the sensor in the measured gas. Selectivity between two gases is defined as the ratio between two responses for different gases. Response time is the period for a sensor to reach 90% of the step value between  $R_{\text{air}}$  and  $R_{\text{gas}}$ . Recovery time is the timeframe for a gas sensor to change back to 90% of the step between  $R_{\text{gas}}$  and  $R_{\text{air}}$ .

The traditional sensing model of MOS CO sensors can be explained in terms of three different aspects, i.e., receptor function, transducer function, and utility factor [31], as seen in Figure 1. The receptor function means an intraparticle model, which is in close relationship to the adsorption and reaction of CO molecules with the oxygen species that is adsorbed onto the surface of the MOS, inducing variation in the width of the space charge layer of the MOS.

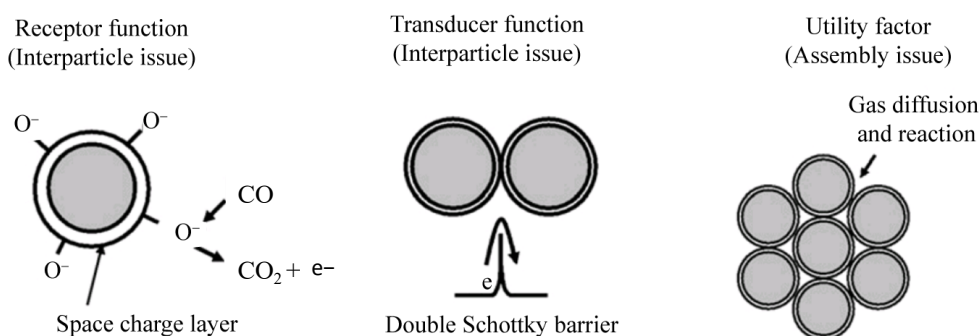


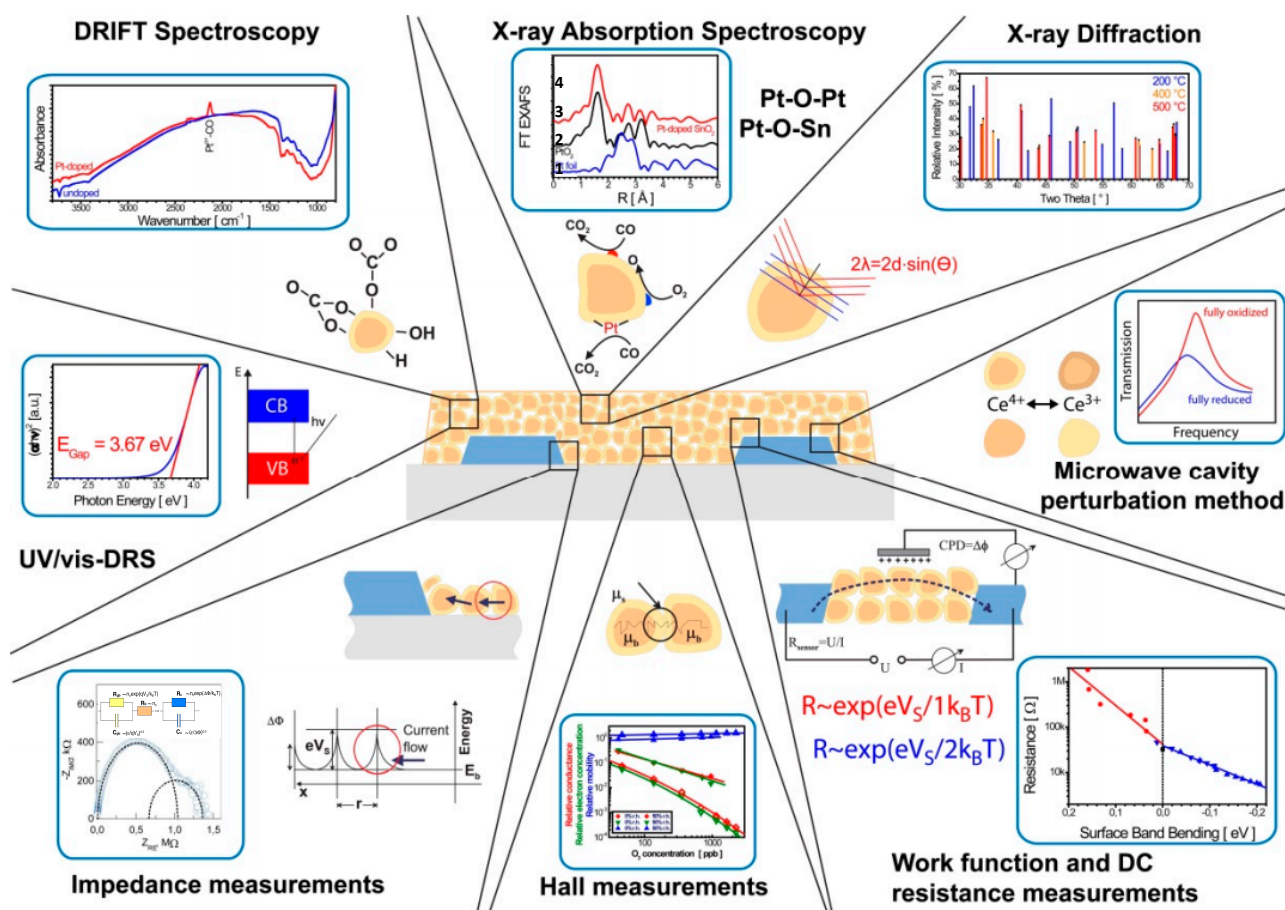
**Figure 1.** Basic sensing model of MOS CO gas sensors. Revised with permission from Ref. [31].

The possible CO sensing mechanism of the MOS is as follows: The oxygen species can be O<sup>2-</sup>, O<sup>-</sup>, or O<sup>2-</sup>, determined by the working temperatures [32]. The following possible reactions between CO and the adsorbed oxygen species will change the resistance of the sensing particles (Table 1). Meanwhile, the transducer function, i.e., interparticle model, is connected to the change in the height of the double Schottky barrier, causing changes in the resistance of the sensors. In addition, the utility factor is an assembly model, which suggests that the sensing characteristics of the MOS are also related to the pore configurations and film thickness of the MOS that determine the diffusion length of CO in the MOS materials. Moreover, water molecules are believed to interact with CO during the room-temperature sensing process as well, which has been studied by Diffuse Reflectance Infrared Fourier Transform Spectroscopy. This will be discussed further below in relation to the SnO<sub>2</sub>-Pd samples.

**Table 1.** Reaction between CO and the oxygen species adsorbed on the surface of MOS at elevated temperatures.

Possible Reaction	Temperature Range	
$2\text{CO} + \text{O}_2^- (\text{ads}) \rightarrow 2\text{CO}_2 + \text{e}^-$	$T < 150\text{ }^\circ\text{C}$	(1)
$\text{CO} + \text{O}^- (\text{ads}) \rightarrow \text{CO}_2 + \text{e}^-$	$150\text{ }^\circ\text{C} \leq T \leq 300\text{ }^\circ\text{C}$	(2)
$\text{CO} + \text{O}^{2-} (\text{ads}) \rightarrow \text{CO}_2 + 2\text{e}^-$	$T > 300\text{ }^\circ\text{C}$	(3)

In situ measurement is very powerful for the investigation of the detailed mechanism of CO sensing [33], as shown in Figure 2. X-ray diffraction and X-ray absorption spectroscopies can be employed to study the structure information of the sensing materials. Diffuse Reflectance Infrared Fourier Transform Spectroscopy (DRIFTS) or Raman spectroscopy can be used to study the surface chemical information of the sensing materials. DRIFTS has been shown to be very effective for studying the sensing mechanism of CO gas based on a MOS. Its advantages include easy operation, direct usage of the sample, and simple sample preparation. Several examples of mechanism study using DRIFTS can be found in the next section.

**Figure 2.** Illustration of in situ spectroscopy for studying the working mechanisms of a MOS for CO sensing [33].

### 3. MOS Sensing Materials

#### 3.1. $\text{SnO}_2$

$\text{SnO}_2$  is the most commonly employed metal oxide for CO detection because of its excellent self-catalysis effect due to its dual valences +2, +4. Its band gap is 3.6 eV. The Fermi level of  $\text{SnO}_2$  is  $-4.7\text{ eV}$  [34]. Generally, it can be produced through the wet or dry method (sputtering or chemical vapor deposition) [32,35–40]. The wet method is more

popular than the sputtering method due to its ability to adjust morphologies in a simple way. For example, the hydrothermal method can produce various morphologies of  $\text{SnO}_2$ , adjusting the CO sensing performance in a large range [41], as seen in Figure 3. At first,  $\text{Sn}^{4+}$  ions and  $\text{OH}^-$  react with each other and form precipitation. Some  $\text{SnO}_2$  nuclei will form from dehydration of the  $\text{Sn}^{4+}$  ions. Next, the small  $\text{SnO}_2$  nuclei will grow bigger. Nanoparticles, nanospheres, nanowires, or nanorods can be obtained by controlling the reactant and additives.

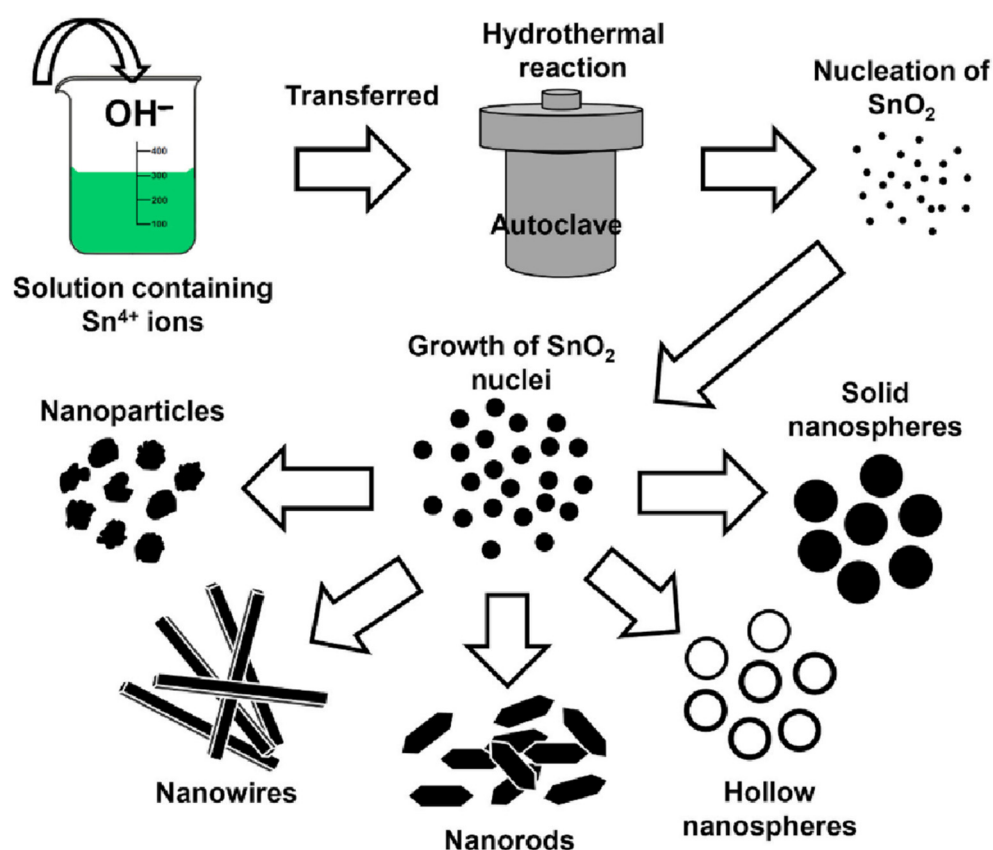


**Figure 3.** Illustration of various  $\text{SnO}_2$  nanostructures using the hydrothermal method [41].

However, pure  $\text{SnO}_2$  is seldom reported to be sensitive to CO at room temperature. Au, Pt, or Pd are usually added to the surface of  $\text{SnO}_2$  to promote room-temperature CO sensing. Table 2 summarizes the comparison of the performance of  $\text{SnO}_2$  composites for room-temperature CO sensing. Nanosized  $\text{SnO}_2$  can be obtained by the hydrothermal method by employing poly ethylene glycol (PEG-6000) [42]. Au impregnation was performed with gold chloride ( $\text{HAuCl}_4 \cdot 3\text{H}_2\text{O}$ ). The optimum Au- $\text{SnO}_2$  sample can respond to 500 ppm CO with a response of about 50 in 20 s. The humidity effect was checked, and the optimum Au- $\text{SnO}_2$  response was almost the same under RH 55% and RH 70%. The mechanisms of room-temperature CO sensing using Au- $\text{SnO}_2$  can be attributed to two aspects: First, Au has a catalytic effect through chemical sensitization via the spillover effect. Second, Au will increase the surface resistance of the Au- $\text{SnO}_2$  composite through the Schottky barrier effect, as discussed by Yamazoe [43].

A comparison of the performance of  $\text{SnO}_2$  composites is shown in Table 2. Pt decoration has been shown to enhance the sensitivity of  $\text{SnO}_2$  to CO, showing a response value of 64.5 to 100 ppm at room temperature [43]. It can be confirmed that both components and structures of  $\text{SnO}_2$  composites can influence the sensing performance of the composites. For example, Pt-doped  $\text{SnO}_2$  porous nanosolid shows a much higher response than that of Pt-doped  $\text{SnO}_2$  nanoparticles [44,45]. The inclusion of perovskite and Pd-Au not only

enhances the response of SnO<sub>2</sub>, but also shortens the response time and recovery time to around 30 s [46].

**Table 2.** Comparison of performance of different SnO<sub>2</sub> composites for CO sensing at room temperature.

Sensing Material	CO Concentration (ppm)	Response	Response Time (s)	Recovery Time (s)	Reference
Au-SnO <sub>2</sub>	500	~50	20 (50 °C)	NA	[42]
Pt-SnO <sub>2</sub> nanoparticle	5000	3.57	~720	NA	[45]
Pt-SnO <sub>2</sub> porous nanosolid	100	64.5	144	882	[44]
Pd-SnO <sub>2</sub> nanoparticle	50	~5	20	40	[47]
Polyaniline-Pd-SnO <sub>2</sub>	300	4	88	62	[48]
CH <sub>3</sub> NH <sub>3</sub> SnI <sub>3</sub> /SnO <sub>2</sub> /Pd/Au	50	68	25	32	[46]
CNT-Co <sub>3</sub> O <sub>4</sub> -SnO <sub>2</sub>	1000	1.46 (V <sub>a</sub> /V <sub>g</sub> )	120	150	[2]

SnO<sub>2</sub> can be doped with Pt by mixing hexachloro-platinic acid (H<sub>2</sub>PtCl<sub>6</sub>) with rutile SnO<sub>2</sub> powder [44]. The samples were sintered at 600, 700, and 800 °C. It was found that heat-treating at 800 °C will lead to grain growth and surface area reduction, thus lowering the sensitivity. The SnO<sub>2</sub>-Pt sample annealed at 700 °C has the highest sensitivity among all the samples. Moreover, 1 wt% Pt-doped SnO<sub>2</sub> powder can respond to 5000 ppm CO with a sensitivity of 3.57. H<sub>2</sub>PtCl<sub>6</sub> was loaded onto SnO<sub>2</sub> porous nanosolid (PNS) as well. The mixture was sintered in nitrogen at a temperature ranging from 400 to 600 °C. It was found that 500 °C is the optimum calcining temperature.

Doped SnO<sub>2</sub> PNS with a 0.5 mm thickness can respond to 100 ppm CO with a sensitivity of 64.5, as shown in Figure 4a. The sensor has excellent selectivity to CO compared to H<sub>2</sub> or CH<sub>4</sub>, as seen in Figure 4b. The mechanism of the excellent CO sensing performance of the Pt-loaded SnO<sub>2</sub> PNS can be explained by the electrical and chemical effects. The electrical effect was further studied by Hall effect measurement. The electron concentration *n* and mobility *μ* before and after exposure to 1000 ppm CO were compared. It was found that the carrier concentration of the best sample increased by almost 50 times after exposure. Meanwhile, the carrier mobility of the best sample increased by 4.76 times after exposure. This phenomenon is in line with the neck control model, i.e., the carrier concentration is determined by the depletion layer and the mobility is controlled by the width of the conduction channel at the grain neck.

As seen in Figure 4c, surface-adsorbed oxygen molecules will change into oxygen ions by drawing electrons from SnO<sub>2</sub>. The oxygen ions will form a depletion layer on the surface of SnO<sub>2</sub>. Pt decoration will promote dissociation of the oxygen molecules, increasing the width of the surface depletion layer, as shown in Figure 4d. When exposed to CO, surface Pt clusters will catalyze the oxidation reaction between the CO and surface-adsorbed oxygen species. The reaction will cause the re-injection of electrons into the SnO<sub>2</sub> nanoparticles. The resistance of the materials will decrease since the width of the conduction channel will be expanded.

Pd-SnO<sub>2</sub> was an excellent candidate for room-temperature CO sensing as well [47]. The sample with a Pd content less than or equal to 2% and heating temperature higher than 1000 °C can respond to 500 ppm CO in 30 s with a response value of 5. The response of the 1 wt% Pd sample heated at 1000 °C to 0.04% CO-N<sub>2</sub> is ten times larger than that to 0.04% CO-20% O<sub>2</sub>-N<sub>2</sub>. This is because that the chemisorption of CO onto SnO<sub>2</sub> will transfer two electrons to SnO<sub>2</sub>. Chemisorption of CO onto SnO<sub>2</sub> will be hindered heavily when oxygen species are present on the surface of SnO<sub>2</sub>. It was confirmed by XRD analysis that PdO forms when the samples are heat-treated at 800 °C, while metallic Pd forms when the samples are heat-treated at 1000 °C instead, as seen in Figure 5a. Furthermore, the XPS results in Figure 5b show that metallic Pd is in the Pd<sup>2+</sup> state for the 5 wt% Pd sample heat-treated at 1000 °C. Figure 5c proves that Pd<sup>2+</sup> and Pd<sup>0</sup> can be found in Pd nanoparticles. Figure 5d shows a pronounced decrease in the Pd<sup>0</sup> ratio in all Pd species, which may be due to electron transfer from Pd to SnO<sub>2</sub> at room temperature. Figure 5e shows that Pd<sup>2+</sup>

and  $\text{Pd}^{4+}$  can be observed in the sample of 1 wt% Pd heat-treated at 1000 °C. It can be concluded from Figure 5b–e that the ratio of Pd to  $\text{SnO}_2$  is crucial for the surface states of Pd. The configurations of the Pd– $\text{SnO}_2$  species are visualized in Figure 5f–h. Three cases are presented: (1) Pd– $\text{SnO}_2$  heated at a temperature lower than 900 °C: PdO was formed on the surface of  $\text{SnO}_2$ , with no response to CO at room temperature; (2) Pd– $\text{SnO}_2$  with Pd content > 2 wt% heated at 1000 °C: Pd was formed on the surface of  $\text{SnO}_2$ , with no response to CO at room temperature; and (3) Pd– $\text{SnO}_2$  with Pd content  $\leq$  2 wt% heated at 1000 °C: Pd was formed on the surface of  $\text{SnO}_2$  with  $\text{Pd}^{4+}$  states, with a response to CO at room temperature. The room-temperature sensing mechanisms of Pd– $\text{SnO}_2$  may be the chemisorption of CO on the Pd nanoparticles at the  $\text{Pd}^{4+}$  sites and the spillover effect of CO toward  $\text{SnO}_2$ .

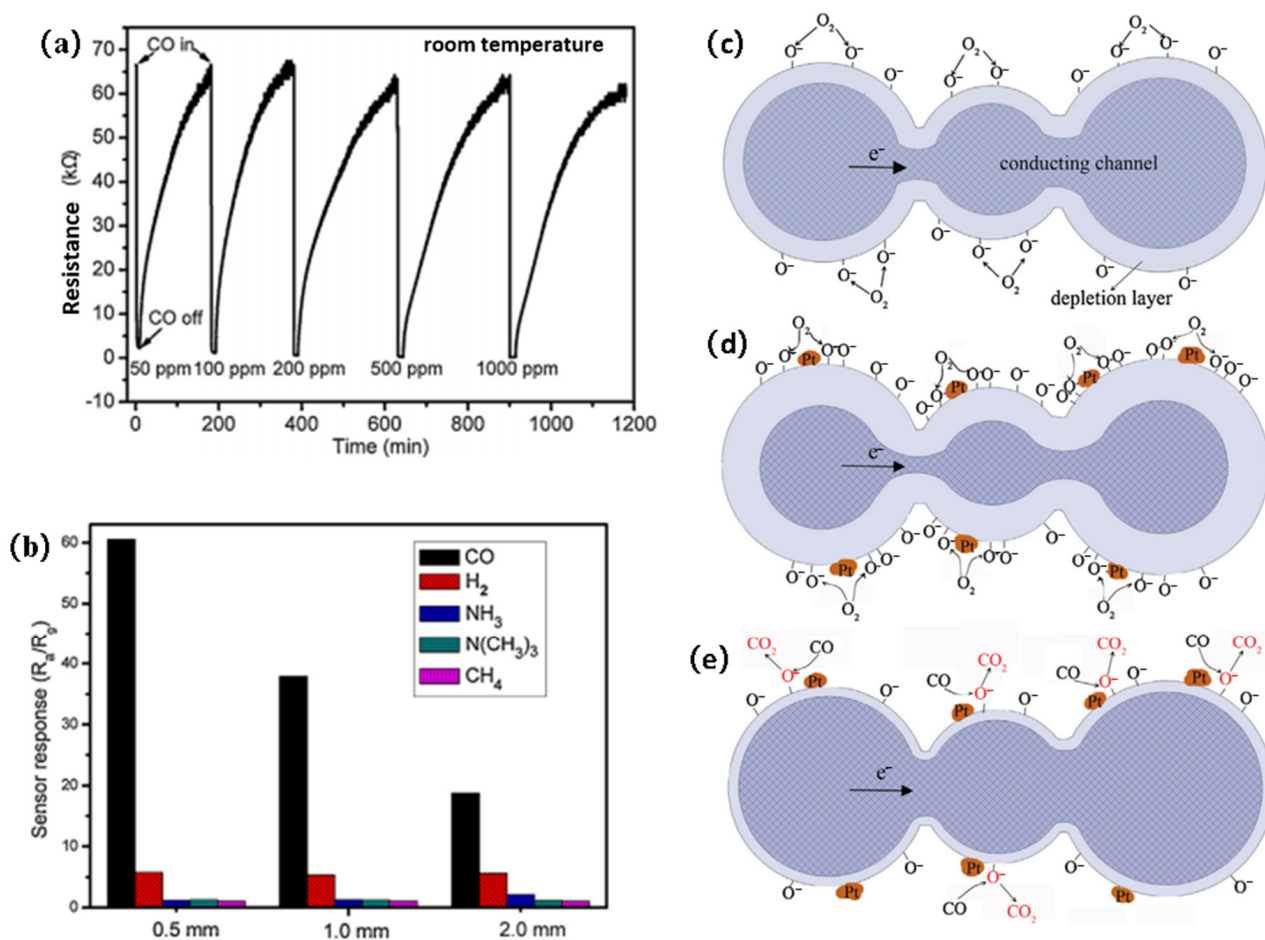


**Figure 4.** (a) Dynamic response curve of the  $\text{SnO}_2$ :Pt PNS sensor to CO at room temperature; thickness of PNS is 0.5 mm. (b) Comparison of response of different  $\text{SnO}_2$ :Pt PNS sensors to 100 ppm CO at room temperature; thickness of PNS is 0.5 mm, 1.0 mm, or 2.0 mm. (c–e) Schematic diagram of the mechanism of the spillover effect that leads to enhancement of the sensing performance of  $\text{SnO}_2$  PNS sensors by Pt-loading: (c) conduction model of  $\text{SnO}_2$  PNS sensor in air; (d) conduction model of  $\text{SnO}_2$ : Pt PNS sensor in air; (e) conduction model of  $\text{SnO}_2$ : Pt PNS sensor in CO [44].

The room-temperature CO sensing mechanisms of PdO-modified  $\text{SnO}_2$  have also been investigated by the DRIFT method. As seen in Figure 6a, the peaks at  $2090\text{ cm}^{-1}$  and  $1840\text{ cm}^{-1}$  only appear for the  $\text{SnO}_2/\text{PdO}_x$  sample [49]. The peaks confirmed the occurrence of CO chemisorption on the reduced Pd species. The first peak refers to linear carbonyl binding to metallic sites with  $\pi$ -back donation from a metal, i.e.,  $\text{Pd}^0$ -bound CO. The other peak corresponds to carbonyls bound to Pd atoms in a bridging configuration. After CO is substituted by air, the strength of the OH stretching band at  $3600\text{--}3200\text{ cm}^{-1}$

declines. This phenomenon is due to the hydrogen bonds between the OH groups. OH species will interact with CO at room temperature following the equation below:

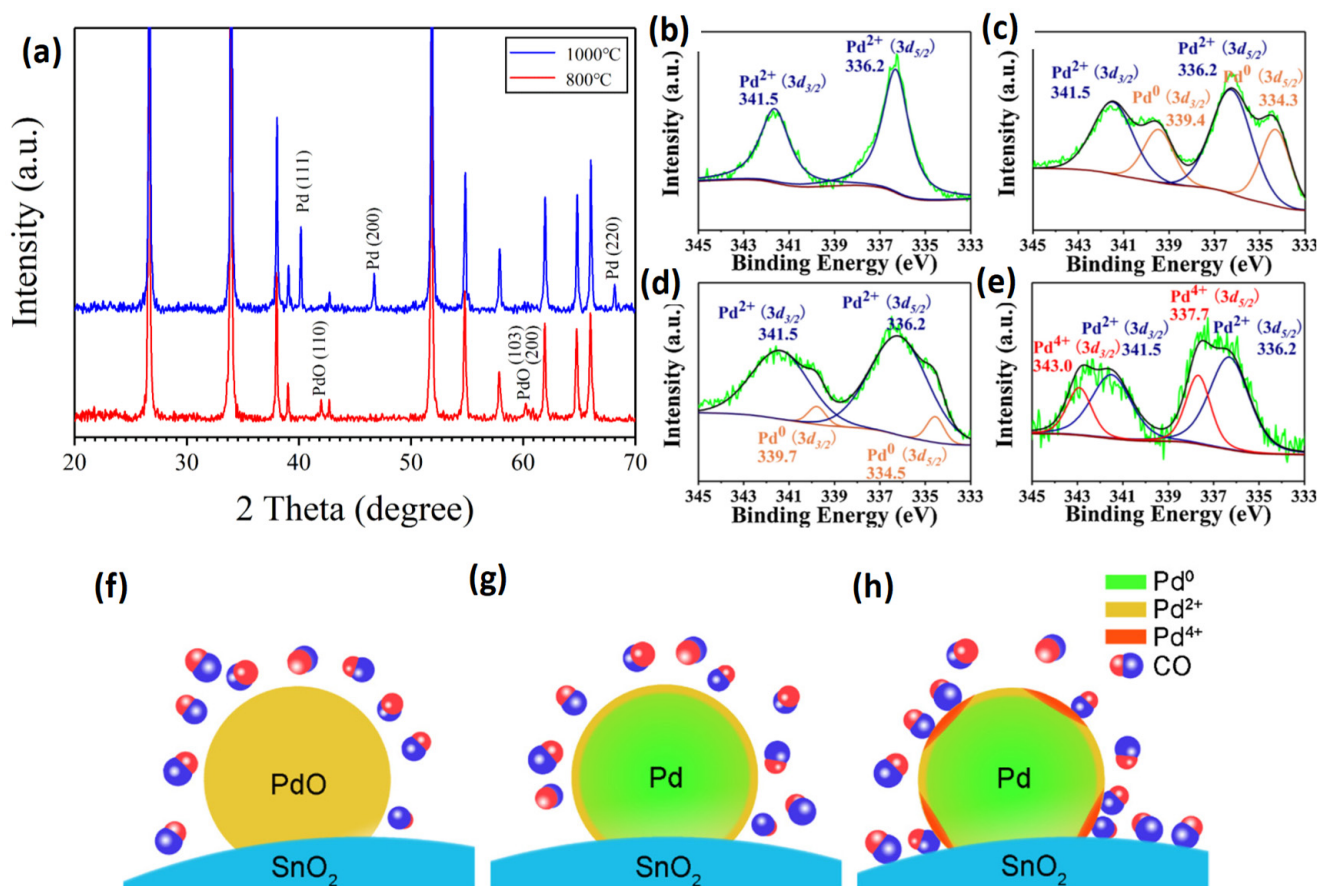


**Figure 5.** (a) XRD patterns for Pd-SnO<sub>2</sub> of 10 wt% Pd heat-treated at 800 °C and 1000 °C, separately. (b–e) XPS spectra of Pd3d<sub>5/2</sub>, 3d<sub>3/2</sub> electrons in different samples: (b) 5 wt% Pd-doped SnO<sub>2</sub> heat-treated at 1000 °C, (c) pure Pd nanoparticles without SnO<sub>2</sub>, (d) a dried nanomixture of both Pd and SnO<sub>2</sub> containing 2 wt% Pd in powder form, (e) 1 wt% Pd-doped SnO<sub>2</sub> heat-treated at 1000 °C. (f–h) Three configurations for Pd-SnO<sub>2</sub> composites and their interactions with CO molecules at room temperature: (f) PdO-SnO<sub>2</sub> composites with no interactions with CO molecules; (g) Pd-SnO<sub>2</sub> composites, whose Pd nanoparticles are in Pd<sup>2+</sup> states on the surface, with no interactions with CO; (h) Pd-SnO<sub>2</sub> composites, whose Pd nanoparticles are in the states of Pd<sup>2+</sup> and Pd<sup>4+</sup> on the surface; in this case, CO molecules are chemisorbed on both Pd<sup>4+</sup> sites of Pd nanoparticles and surface of SnO<sub>2</sub> [47].

As shown in Figure 7a, first tin dioxide nanoparticles were obtained by the hydrothermal and drying method [50]. Then, graphene in different amounts was dispersed in ethanol and then sonicated. Then, 1 g tin oxide was added into the dispersion solution. The 0.5 wt% graphene-decorated SnO<sub>2</sub> has the highest response to 40 ppm CO, as shown in Figure 7b. The 0.5 wt% graphene-decorated SnO<sub>2</sub> can also respond to and recover from 40 ppm CO in less than 45 s, as shown in Figure 7c.

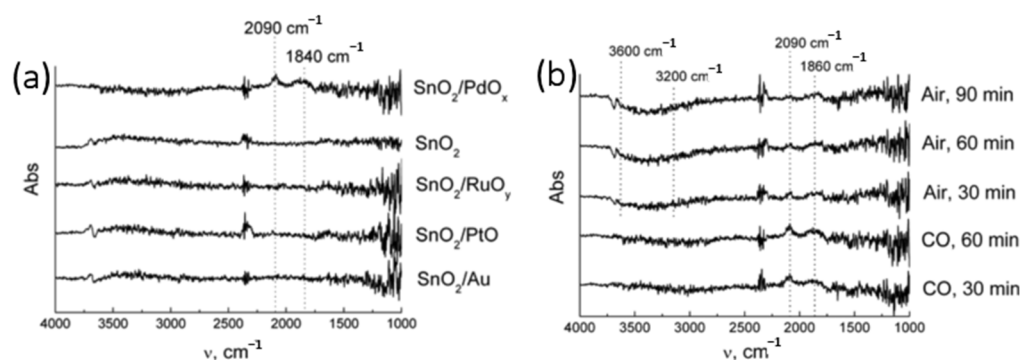


**Figure 6.** DRIFT spectra of SnO<sub>2</sub> and its composites exposed to CO at 25 °C: (a) nanocrystalline SnO<sub>2</sub>/PdO<sub>x</sub>, SnO<sub>2</sub>, SnO<sub>2</sub>/RuO<sub>y</sub>, SnO<sub>2</sub>/PtO, and SnO<sub>2</sub>/Au powders exposed to 100 ppm of CO for 1 h. (b) SnO<sub>2</sub>/PdO<sub>x</sub> powder exposed to 100 ppm of CO and air in sequence for different periods [49].

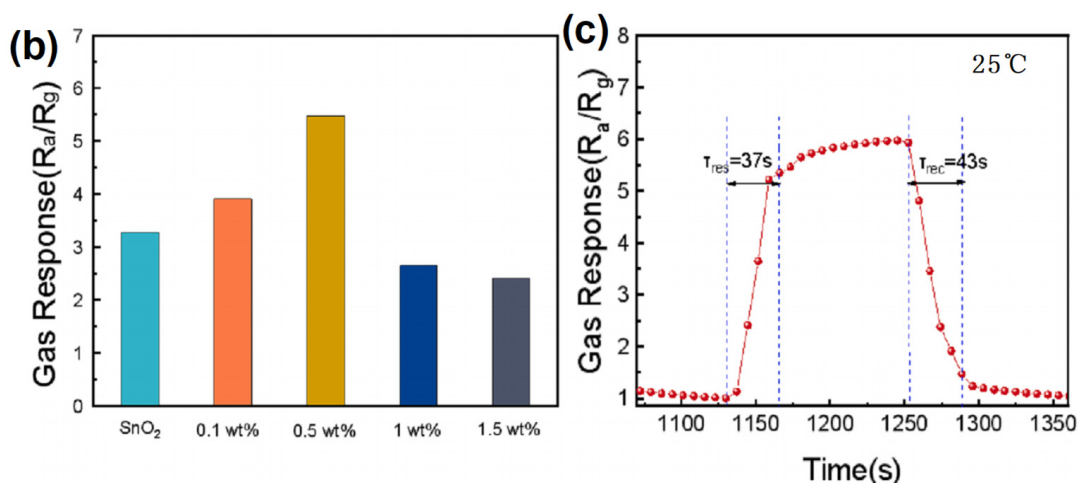
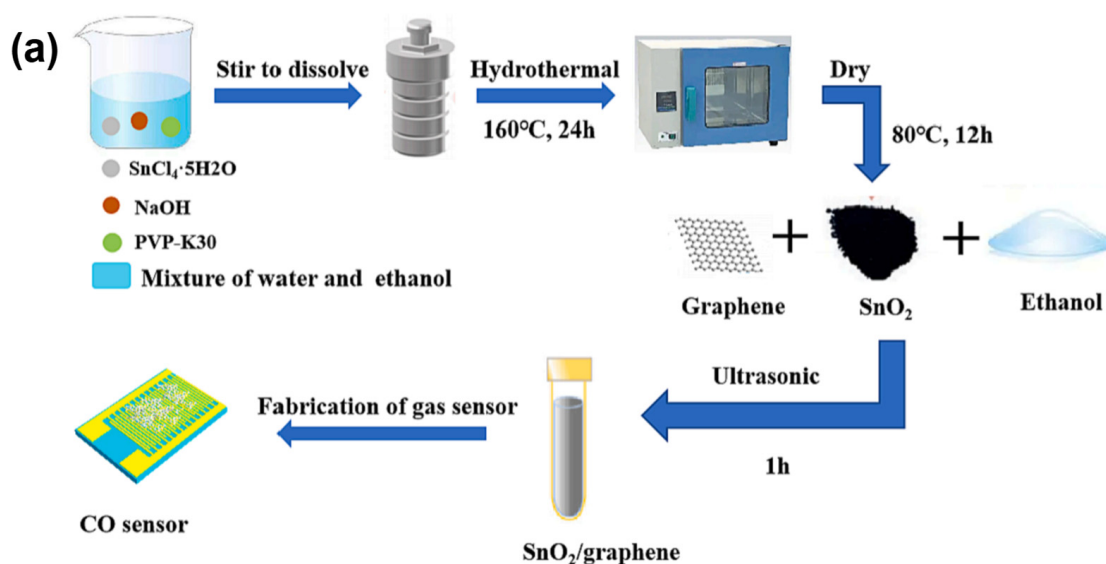


**Figure 7.** (a) The procedure of the fabrication process of CO sensors based on tin dioxide–graphene composites; (b) response of different tin dioxide samples to 40 ppm CO, different colours corresponds to different samples; (c) response and recovery curves of tin dioxide–graphene 0.5 wt% to 40 ppm CO at 25 °C [50].

### 3.2. ZnO

ZnO is one of the most commonly employed CO sensing materials because of its variable morphologies and easy doping processes [51]. Compared to other semiconductor materials, ZnO has many excellent properties, such as a simple synthesis, wide bandgap of 3.37 eV, and binding energy of exciton of 60 meV [52–54]. ZnO can be grown in a controlled manner by the sputtering, CVD, or solution method, of which the solution method is the most popular [54–56]. For example, ZnO nanorods can be formed using  $\text{Zn}(\text{OH})_4^{2-}$  and CTAB aqueous solutions, in which CTAB functions as a structure director [57]. A ZnO nanorod array was realized on a (100) silicon wafer on a 5 nm thick ZnO seed layer by sputtering using ammonia and zinc chloride solution [58]. ZnO hierarchical nanostructures can be grown using sequential nucleation and growth methods [59,60]. The comparison of the performance of various ZnO materials is shown in Table 2. For example, ZnO nanocomb can be synthesized by chemical vapor deposition first. Then, the nanocomb can be drop-casted on  $\text{SiO}_2$ -p-Si substrate with a patterned Ti/Au electrode array on top. The sample can respond to CO at room temperature [61]. In addition, ZnO thin films and nanoneedles are reported to be able to respond to CO at room temperature as well [62]. Au decoration with gold chloride solution,  $\text{HAuCl}_4$ , is an effective way to synthesize Au-ZnO composites for room-temperature CO sensing. Table 3 shows that the base material, ZnO, can finally determine the sensing performance of two similar samples, such as the response time after a comparison of two Au-ZnO samples in [63,64].

**Table 3.** Comparison of performance of ZnO composites for room-temperature CO sensing.

Sensing Material	CO Concentration (ppm)	Response	Response Time (s)	Recovery Time (s)	Reference
ZnO nanocomb	250	7.22	200	50	[61]
ZnO thin films	50	1.10	~180	-	[65]
ZnO nanoneedles	375	1.51	186	38	[62]
Au-ZnO nanowires	100	~5	-	-	[63]
Au-ZnO nanostars	500	55.3	41	40	[64]
$\text{SnSe}_2$ -ZnO polyhedron	200	1.17	19	13	[66]
Pt-ZnO-CuO	1000	2.64	81	81	[67]

Notably, Au-ZnO nanostars can respond to 500 ppm CO in 41 s with a response value over 55 under dynamic mode, which is the highest response value of ZnO room-temperature sensing materials [64]. This high response is due to three aspects (Figure 8): Firstly, the ZnO nanostars are composed of many ultrafine nanoparticles with a typical size of around 20 nm, which offers more reaction sites for adsorption of oxygen. Secondly, the spillover effect of gold nanoparticles can facilitate dissociation of oxygen molecules over ZnO, decreasing the CO sensing temperature. It is believed that this chemical sensitization function should be the predominant mechanism for room-temperature CO sensing of Au-ZnO. The third effect is the work function modulation through the creation of a nanoscopic depletion region at the Au-ZnO surface, altering the Schottky barrier height, as seen in Figure 8b. In addition, ZnO-SnSe<sub>2</sub> was reported to sense CO at room temperature with excellent resistance to humidity interference [66]. The author also found that UV illumination can improve the sensitivity of the material. This phenomenon is similar to that of the MoS<sub>2</sub> composite, which will be discussed further below.

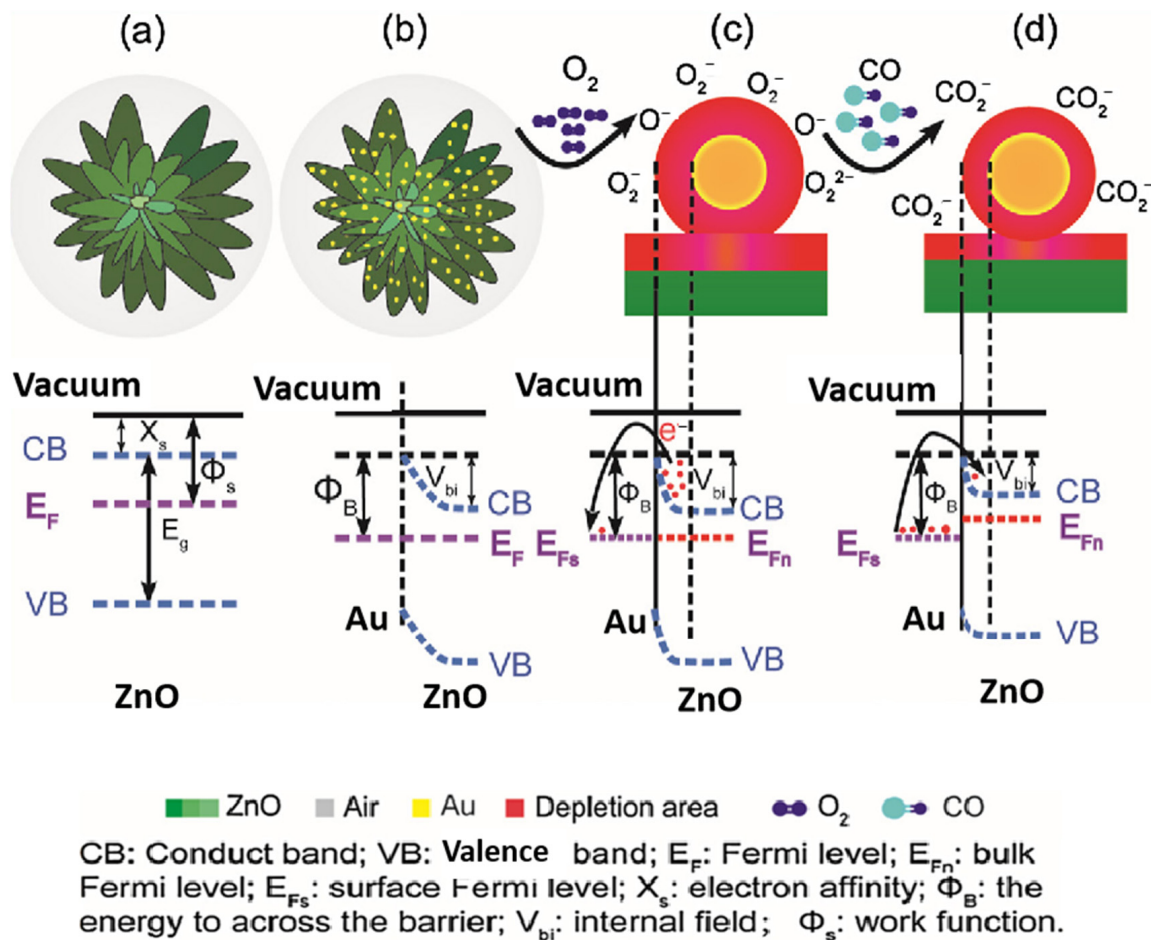


**Figure 8.** Energy band diagram of ZnO and its composites: (a,b) before exposure to oxygen: (a) ZnO nanostars, (b) ZnO nanostars with Au nanoparticles; (c) ZnO nanostars with Au nanoparticles exposed to oxygen; (d) ZnO nanostars with Au nanoparticles with surface-adsorbed oxygen species exposed to CO [64].

### 3.3. Other Metal Oxides

Besides  $\text{SnO}_2$  and ZnO, CuO, doped  $\text{TiO}_2$ , and other metal oxides have been reported to respond to CO at room temperature.  $\text{TiO}_2$  is another interesting sensing material for room-temperature CO sensing.  $\text{TiO}_2$  was widely employed for photocatalysis at the beginning. Solution growth of  $\text{TiO}_2$  can be well controlled through the organic capping method [68]. Later,  $\text{TiO}_2$  nanotubes were synthesized by electrochemical anodization and employed for sensing CO, ethanol, and hydrogen [69]. Moreover, porous  $\text{TiO}_2$  was reported to be suitable for chemical sensors in cyber chemical systems [70]. The latest progress in  $\text{TiO}_2$  nanostructures for gas sensing can be found in another review [71].  $\text{WO}_3$  is an excellent material for CO sensing as well [72,73]. It was reported that  $\text{CeO}_2$ - $\text{WO}_3$  can respond to CO very well at 430 °C. The response and recovery time of the sensor is less than 60 s [74]. Nanocomposites of graphene and  $\text{WO}_3$  can respond to 10 ppm CO at room temperature with a low response value of 1.03. The graphene- $\text{WO}_3$  nanocomposites can respond to 100 ppm CO at 300 °C with a response value of 21.5 under dynamic mode [75]. The comparison of the performance of temperature sensors based on other metal oxides is shown in Table 4.

**Table 4.** Comparison of performance of composites of other materials for room-temperature CO sensing.

Sensing Material	CO Concentration (ppm)	Response	Response Time (s)	Recovery Time (s)	Reference
Pt-Co <sub>3</sub> O <sub>4</sub> -In <sub>2</sub> O <sub>3</sub>	5	4	NA	NA	[76]
Dumbbell CoOOH nanostructures	50	NA	~20	~18	[77]
Fe-TiO <sub>2</sub>	100	~4.8	43	25	[78]
Atomically dispersed Pd-TiO <sub>2</sub>	100	125.49	28	70	[79]
Self-doped Ti <sup>3+</sup> -porous TiO <sub>2</sub>	5000	~2	~10	~30	[80]
Mg-TiO <sub>2</sub> thin films	120	8.40(CO+Ar)	62	30	[81]
CuO-TiO <sub>2</sub> heterojunction	1	~2.2	NA	NA	[82]
CuO (111) nanosheets	100	39.6	100	72.4	[83]
RuO <sub>x</sub> (OH) <sub>y</sub>	250	~2	NA	NA	[84]

Recently, Xu synthesized atomically dispersed Pd over TiO<sub>2</sub> nanoflower through a simple and mild photochemical method at room temperature [79]. SEM of Pd<sub>1</sub>-TiO<sub>2</sub> shows a nanoflower morphology, as seen in Figure 9a. Figure 9b shows that no Pd nanoparticles can be found in Pd<sub>1</sub>-TiO<sub>2</sub>. An interplanar spacing of 0.35 nm is assigned to (100) of TiO<sub>2</sub>. As seen in Figure 9d, 336.2 and 341.4 eV of Pd<sub>1</sub>-TiO<sub>2</sub> belong to Pd<sup>2+</sup> and Pd<sup>0</sup>, indicating partial oxidation of Pd atoms. Figure 9e suggests that the Pd species is in the form of isolated single atoms. Figure 9f shows the uniform distribution of Ti, O, and Pd on nanoflowers.

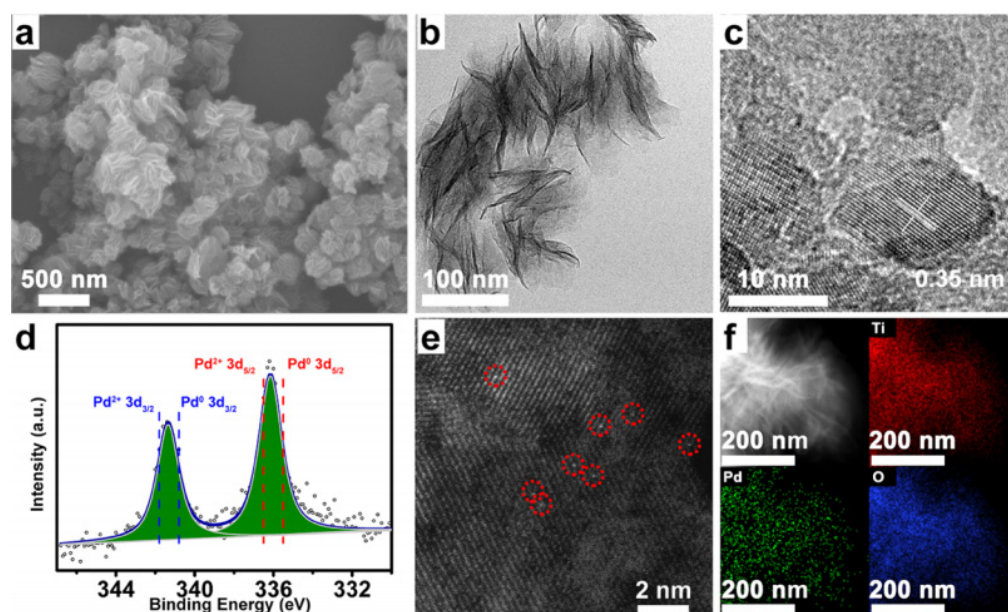


**Figure 9.** Characterization results of the Pd<sub>1</sub>-TiO<sub>2</sub> sample: (a–c) SEM, TEM, and high-resolution TEM images; (d) deconvoluted narrow-scan Pd 3d XPS spectrum; (e) ac-HAADF-STEM image, where the red circle shows that Pd species are in the form of isolated single atoms; and (f) STEM-EDS elemental mapping images [79].

The TiO<sub>2</sub>, Pd NPs-TiO<sub>2</sub>, and Pd<sub>1</sub>-TiO<sub>2</sub> samples all presented a P-type nature according to the analysis results from the UPS and UV-vis spectra. Thus, the oxygen molecules adsorbed on these materials will increase the densities of holes and increase the conductivity. When exposed to CO as a reductive analyte, free electrons will be injected into the materials and decrease the conductivity. O<sub>ads</sub> refers to the adsorbed active oxygen species, i.e., mainly O<sub>2</sub><sup>-</sup> at room temperature. The relative percentage of O<sub>ads</sub> increased from 8.02% to 52.12% for TiO<sub>2</sub> and Pd<sub>1</sub>-TiO<sub>2</sub> (Figure 10b). Figure 10c shows that the CO adsorption ability is in the order TiO<sub>2</sub> < Pd NPs-TiO<sub>2</sub> < Pd<sub>1</sub>-TiO<sub>2</sub>. Meanwhile, the adsorption intensity of CO<sub>2</sub> production of Pd<sub>1</sub>-TiO<sub>2</sub> is greater than that of Pd NPs-TiO<sub>2</sub>, revealing higher

room-temperature CO oxidation efficiency. Furthermore, the adsorption energy of CO on Pd<sub>1</sub>-TiO<sub>2</sub> is -0.77 eV, which is the lowest among all the calculated gases, and accounts for the high selectivity of the sample to CO (Figure 10d).

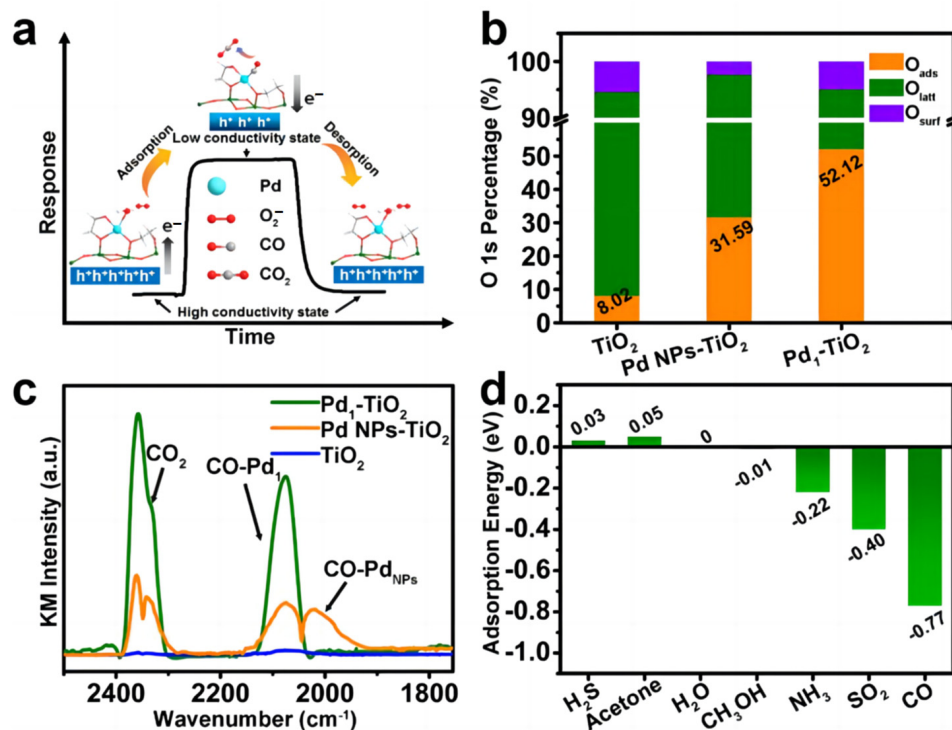


**Figure 10.** (a) Proposed CO sensing mechanism of Pd<sub>1</sub>-TiO<sub>2</sub>. (b) Relative percentages of O species from O 1s spectra of TiO<sub>2</sub> nanoflowers, Pd NPs-TiO<sub>2</sub>, and Pd<sub>1</sub>-TiO<sub>2</sub>. (c) DRIFT spectra of TiO<sub>2</sub> nanoflowers, Pd NPs-TiO<sub>2</sub>, and Pd<sub>1</sub>-TiO<sub>2</sub>. (d) Calculated adsorption energies of selected gases on Pd<sub>1</sub>-TiO<sub>2</sub> [79].

### 3.4. Metal Oxide–2D Material Composites

Two-dimensional materials are very absorbing due to their unique structures and electronic properties. MoS<sub>2</sub> is widely applied in room-temperature gas sensing materials [85,86]. It has many excellent properties, such as the very high luminescence quantum efficiency of single-layer MoS<sub>2</sub>. MoS<sub>2</sub> has already been used for room-temperature sensing H<sub>2</sub>S, NO<sub>2</sub>, and SO<sub>2</sub> [87–91]. Recently, several works have been reported regarding room-temperature CO sensing based on MoS<sub>2</sub>-MOS composites. For example, Ag-ZnO-MoS<sub>2</sub> was prepared by the layer-by-layer (LBL) self-assembly method [92]. The sample can respond to 100 ppm CO with a response value of 1.05. Both the response and recovery processes take less than 60 s. This fast process under room temperature is due to the catalytic effect of Ag and synthetic effect of ZnO and MoS<sub>2</sub>. Co-In<sub>2</sub>O<sub>3</sub>-MoS<sub>2</sub> can be prepared by LBL self-assembly as well [93]. The sample can achieve a response value of 1.08 to 10 ppm CO in 39 s. It is the Co<sup>2+</sup> doping and heterojunction formation from both Co-In<sub>2</sub>O<sub>3</sub> and MoS<sub>2</sub> that contributes to the excellent CO sensing behavior. Moreover, SnO<sub>2</sub>-MoS<sub>2</sub> was reported to respond to 40 ppm CO at room temperature with a response value of 4.97 under UV light illumination [94]. The sensing mechanism is shown in Figure 11. First, MoS<sub>2</sub> can prevent interparticle aggregation of SnO<sub>2</sub> nanoparticles and provide more sites for the adsorption of CO molecules from SnO<sub>2</sub>, thus increasing the sensitivity. Moreover, MoS<sub>2</sub> provides direct conduction paths for charge carriers, because of its high charge carrier mobility. Moreover, MoS<sub>2</sub> and SnO<sub>2</sub> can form a p-n junction that can improve the electron-hole separation under UV irradiation.

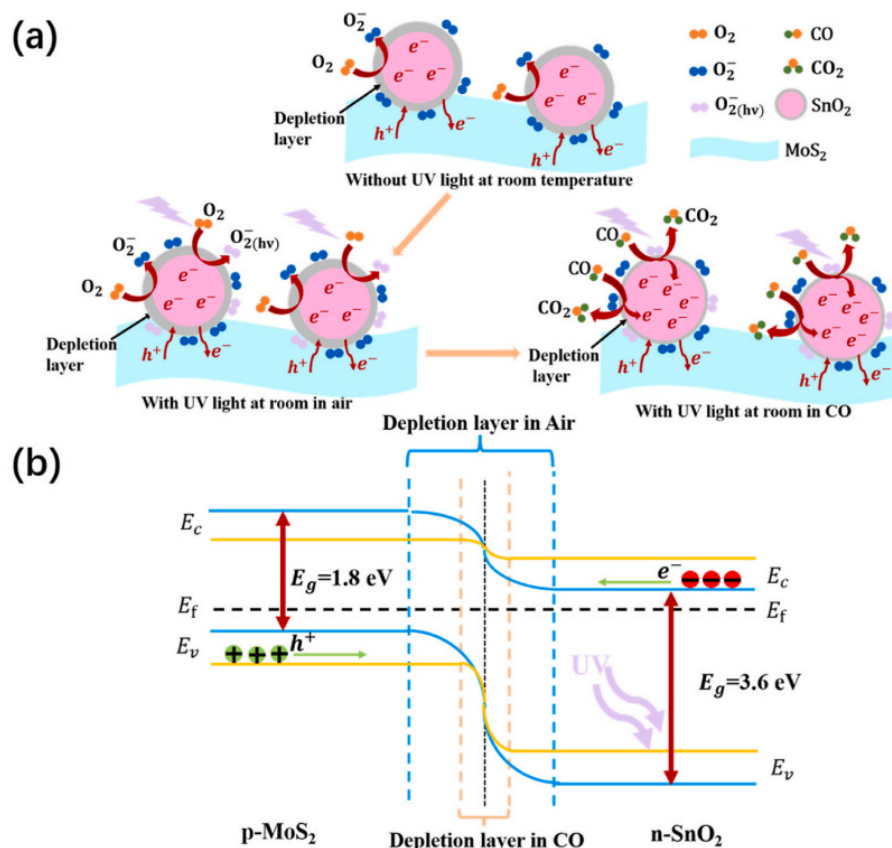
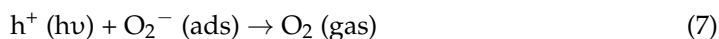
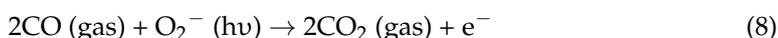


**Figure 11.** Illustration of the working mechanism of MoS<sub>2</sub>/SnO<sub>2</sub> response to CO under UV light. (a) Changes in surface element during the sensing step with or without UV; (b) band diagram between p-MoS<sub>2</sub> and n-SnO<sub>2</sub> [94].

When UV light is employed, the photogenerated electron–hole pairs are excited and separated by the built-in electric fields in SnO<sub>2</sub>. The photogenerated electrons on the conduction band of MoS<sub>2</sub> can readily be transferred to SnO<sub>2</sub>, and the photogenerated holes on the valence band of SnO<sub>2</sub> can be transferred to MoS<sub>2</sub>. The photogenerated electrons will then be captured by O<sub>2</sub> and yield new O<sup>2−</sup>. Simultaneously, the reaction of the photogenerated holes with the adsorbed oxygen ions on the surface of the sensing material occurs according to Equations (5) and (6) shown below:



The photogenerated electron hole can be separated efficiently at the interface, preventing recombination and enhancing the sensing performance. Once SnO<sub>2</sub> is exposed to CO gas, CO adsorbed on the surface of SnO<sub>2</sub> can also react with photogenerated electrons, as seen in Equation (8):



In addition, a SnO<sub>2</sub>-MoSe<sub>2</sub> nanoflower was synthesized through the hydrothermal method. The composite can respond to 1 ppm CO very quickly, with higher sensitivity than the pristine MoSe<sub>2</sub> or SnO<sub>2</sub>. The sensing mechanism may be the formation of n-n junctions between n-type SnO<sub>2</sub> and n-type MoSe<sub>2</sub> [95]. A comparison of MoS<sub>2</sub> composites for room-temperature CO sensors can be found in Table 5.

**Table 5.** Comparison of performance of composites of MoS<sub>2</sub> for room-temperature CO sensing.

Sensing Material	CO Concentration (ppm)	Response	Response Time (s)	Recovery Time (s)	Reference
Ag-ZnO-MoS <sub>2</sub>	100	1.05	45	40	[92]
Co-In <sub>2</sub> O <sub>3</sub> -MoS <sub>2</sub>	10	1.08	~39	~18	[93]
SnO <sub>2</sub> -MoS <sub>2</sub> UV	40	4.97	43	36	[94]

#### 4. Discussion of Sensing Mechanism

The CO sensing mechanisms of MOSs at temperatures higher than room temperature have been reported in several papers already [96–98]. While a precise understanding of the CO sensing mechanisms of MOSs at room temperature is still in its early stages, a general model can be deduced from the works reported already. Below are some critical factors:

##### (1) Structures of MOS nanostructures

The structure (crystal plane, grain size, morphology, and so on) of the sensing materials will significantly influence the sensing performance. On one hand, MOSs with smaller grain size will usually have a higher response to CO at room temperature, which is in line with the grain size sensing model in Figure 3. For example, the ZnO thin films with the smallest grain size among all three types of samples have the highest response to CO at room temperature [65]. In addition, specific crystal planes and more active defects can enhance CO sensing at room temperature. For instance, it was reported that CuO nanosheets with exposed (111) crystal facets and more oxygen vacancies have a higher response to and lower detection limit of CO at room temperature.

##### (2) Surface modification of MOSs

There are two main surface modification methods for MOSs, i.e., doping of noble metals or formation of heterojunctions. Doping of noble metals is the most common method to enhance room-temperature CO sensing based on MOSs. The chemical sensitization effect is the main contributing factor in lowering the working temperature. The chemical states and dispersion states of noble metals on the surface of a MOS play a vital role in its CO sensing performance at room temperature, as shown in the case of the Pd-MOS system [47]. In addition, a heterojunction of a MOS will enhance the room-temperature CO sensing at both the receptor and transducer point. For example, CuO-TiO<sub>2</sub> composite can respond to CO at room temperature [82]. CuO materials have excellent CO adsorption properties, enhancing the receptor performance of the composites. Moreover, CuO-TiO<sub>2</sub> can form a p-n junction, creating a space charge region at the interface of the two materials.

##### (3) Annealing effect

The annealing effect, like the annealing atmosphere and annealing temperature, can also influence the room-temperature CO sensing performance of the MOS material. Considering SnO<sub>2</sub>-Pt composites, the SnO<sub>2</sub>-Pt composite annealed in nitrogen has a much higher response than that annealed in air [44]. The reason is twofold: First, the atmosphere can determine the chemical state of the loaded Pt. More Pt<sup>2+</sup> with a much higher catalyzing activity will be present in SnO<sub>2</sub>-Pt annealed in nitrogen. Second, SnO<sub>2</sub>-Pt annealed in nitrogen has more oxygen vacancies that can be sites for chemisorption of oxygen. Furthermore, higher annealing temperatures can increase the crystallinity of the sensing material, as they did in Au-In<sub>2</sub>O<sub>3</sub> [99]. However, too high a temperature, like 600 °C, may destroy the nanorod and make Au agglomerate in Au-In<sub>2</sub>O<sub>3</sub>.

##### (4) UV activation

UV activation on the photosensitive materials will generate more electrons, thus forming more O<sub>2</sub><sup>-</sup> at the surface, enhancing the reaction between oxygen species and CO at room temperature. For example, ZnO and TiO<sub>2</sub> are very sensitive to UV light. MoS<sub>2</sub> and SnSe<sub>2</sub> have higher sensing performance under UV as well [95].

## 5. Conclusions

In this review, the typical studies of MOSs for room-temperature CO sensors have been summarized and discussed. For example, noble metal-doped SnO<sub>2</sub> can function well for room-temperature CO sensing. ZnO with smaller diameters can sense CO at room temperature. Self-doped or Pd-doped TiO<sub>2</sub> can respond to CO very well at room temperature as well. The room-temperature CO sensing mechanism of MOSs can be categorized into four parts: the structures of MOSs, surface modification effects, UV activation, and the annealing effect. MOSs with a smaller diameters usually have better CO sensing performance at room temperature. A noble metal or heterojunction effect at the surface of MOSs can facilitate room-temperature CO sensing. Moreover, UV activation can promote room-temperature CO sensing in some materials such as ZnO, TiO<sub>2</sub>, or MoS<sub>2</sub>. Both the annealing atmosphere and temperature can effect room-temperature CO performance. The future characteristics of room-temperature CO sensors will be higher sensitivity, a lower detection limit and cost, and a smaller size for integration and portable devices. Combining material engineering and MEMS technology is another promising field. This review will be of interest to many researchers and engineers working on sensor materials or in the safety monitoring sensor field.

**Author Contributions:** Conceptualization, Y.H. and M.J.; validation, Y.H.; formal analysis, Y.H.; investigation, M.J.; resources, Y.H.; data curation, M.J.; writing—original draft preparation, M.J.; writing—review and editing, Y.H.; visualization, M.J.; supervision, M.J.; funding acquisition, Y.H. All authors have read and agreed to the published version of the manuscript.

**Funding:** This research was funded by the International Science and Technology Cooperation Project of Tiandi Technology Co., Ltd. (No. 021-2-GH003), Key Technology and Standards of Mine Internet of Things of Tiandi Technology Co., Ltd. (No. 2019-TD-ZD007), and National Science Foundation Council (62204260).

**Institutional Review Board Statement:** Not applicable.

**Informed Consent Statement:** Not applicable.

**Data Availability Statement:** No new data were created or analyzed in this study. Data sharing is not applicable to this article.

**Conflicts of Interest:** Author Yaoyi He employed by the company Tiandi (Changzhou) Automation Co., Ltd. The remaining authors declare that the research was conducted in the absence of any commercial or financial relationships that could be construed as a potential conflict of interest.

## References

1. Choi, S.W.; Kim, J.; Lee, J.H.; Byun, Y.T. Remarkable Improvement of CO-Sensing Performances in Single-Walled Carbon Nanotubes Due to Modification of the Conducting Channel by Functionalization of Au Nanoparticles. *Sens. Actuators B Chem.* **2016**, *232*, 625–632. [[CrossRef](#)]
2. Wu, R.J.; Wu, J.G.; Yu, M.R.; Tsai, T.K.; Yeh, C.T. Promotive Effect of CNT on Co<sub>3</sub>O<sub>4</sub>-SnO<sub>2</sub> in a Semiconductor-Type CO Sensor Working at Room Temperature. *Sens. Actuators B Chem.* **2008**, *131*, 306–312. [[CrossRef](#)]
3. Roy, A.; Ray, A.; Sadhukhan, P.; Naskar, K.; Lal, G.; Bhar, R.; Sinha, C.; Das, S. Polyaniline-Multiwalled Carbon Nanotube (PANI-MWCNT): Room Temperature Resistive Carbon Monoxide (CO) Sensor. *Synth. Met.* **2018**, *245*, 182–189. [[CrossRef](#)]
4. Wang, H. Research Progress of Low-Power Carbon Monoxide Sensor. *Ind. Mine Autom.* **2021**, *47*, 16–23. [[CrossRef](#)]
5. Dong, K.N.; Yang, J.F. Development of Mine-Used Infrared Carbon Monoxide Sensor Based on Mini Pump Suctio. *Ind. Mine Autom.* **2021**, *47*, 128–132.
6. Shrivastava, S.; Mahana, D.; Nehra, S.; Gangwar, S.; Singh, S.; Yadav, C.S.; Muthusamy, S.K.; Dogra, A. CO Gas Sensing Characteristics of BaSnO<sub>3</sub> Epitaxial Films Prepared by PLD: The Effect of Film Thickness. *Sens. Actuators B Chem.* **2024**, *400*, 134882. [[CrossRef](#)]
7. Ani, A.; Poornesh, P.; Antony, A.; Chattopadhyay, S. Synergism of Spray-Pyrolyzed Aliovalent Ga (Iii) Ions and ZnO Nanostructures for Selective Sensing of Hazardous CO Gas towards Low Ppm Levels. *Sens. Actuators B Chem.* **2024**, *399*, 134827. [[CrossRef](#)]
8. Zegebreal, L.T.; Tegegne, N.A.; Hone, F.G. Recent Progress in Hybrid Conducting Polymers and Metal Oxide Nanocomposite for Room-Temperature Gas Sensor Applications: A Review. *Sens. Actuators A Phys.* **2023**, *359*, 114478. [[CrossRef](#)]

9. Desimone, P.M.; Zonta, G.; Giulietti, G.; Ortega, P.P.; Aldao, C.M.; Simões, A.Z.; Moura, F.; Ponce, M.A.; Foschini, C.R. Towards Carbon Monoxide Detection Based on ZnO Nanostructures. *Mater. Sci. Eng. B* **2024**, *299*, 117003. [\[CrossRef\]](#)
10. Sadredini, A.R.; Nikfarjam, A.; Naeimi Pour, M.; Nazeri, N. Intensity Modulation of UV Light in Gas Sensor Array to Discriminate Several Analytes at Room Temperature. *IET Sci. Meas. Technol.* **2023**, *18*, 65–73. [\[CrossRef\]](#)
11. Tang, M.; Zhang, D.; Sun, Y.; Chen, Q.; Chen, Y.; Xi, G.; Wang, Z.; Shao, X. CVD-Fabricated Co<sub>3</sub>O<sub>4</sub>-Co<sub>3</sub>S<sub>4</sub> Heterojunction for Ultra-Sensitive Detection of CO in SF<sub>6</sub> Discharge Decomposition Products. *Sens. Actuators B Chem.* **2024**, *401*, 134968. [\[CrossRef\]](#)
12. Chen, M.; Li, X.; Li, Y.; Li, Y.; Qin, Z.; Wang, Q. MOF-Derived Co<sub>3</sub>O<sub>4</sub> Nanoparticles over Direct Grown ZnO Nanoflower on Ceramic for CO Sensor with High Selectivity. *Sens. Actuators B Chem.* **2024**, *401*, 134951. [\[CrossRef\]](#)
13. de Araújo, E.P.; Paiva, M.P.; Moisés, L.A.; Santo, G.S.D.E.; Blanco, K.C.; Chiquito, A.J.; Amorim, C.A. Improving Hazardous Gas Detection Behavior with Palladium Decorated SnO<sub>2</sub> Nanobelts Networks. *Sensors* **2023**, *23*, 4783. [\[CrossRef\]](#) [\[PubMed\]](#)
14. Zhao, F.; Cao, W.; Wang, P.H.; Wang, J.; Yu, L.; Qiao, Z.; Ding, Z.J. Fast and Sensitive Detection of CO by Bi-MOF-Derived Porous In<sub>2</sub>O<sub>3</sub>/Fe<sub>2</sub>O<sub>3</sub> Core-Shell Nanotubes. *ACS Sens.* **2023**, *8*, 4577–4586. [\[CrossRef\]](#) [\[PubMed\]](#)
15. Ali, Z.M.; Murshed, M.N.; El Sayed, M.E.; Samir, A.; Alsharabi, R.M.; Farea, M.O. A New Fabrication Strategy of Ag<sub>2</sub>O Doped PANI as a Highly Stable and Room Temperature Operable Carbon Monoxide Gas Sensor. *Opt. Mater.* **2023**, *144*, 114324. [\[CrossRef\]](#)
16. Al-Maamori, M.H.; Al-Jamal, A.N.; Habeeb, S.A.; Hassan, A.S.; Majdi, H.S. Al<sup>3+</sup>-Modified ZnO Thin Film Sensor Fabricated by the Sputtering Method: Characterization and a Carbon Monoxide Gas Detection Study. *J. Chem. Res.* **2024**, *48*, 17475198231221453. [\[CrossRef\]](#)
17. Meng, F.J.; Guo, X.M. Co/Au Bimetal Synergistically Modified SnO<sub>2</sub>-In<sub>2</sub>O<sub>3</sub> Nanocomposite for Efficient CO Sensing. *Ceram. Int.* **2023**, *49*, 15979–15989. [\[CrossRef\]](#)
18. You, S.; Li, G.; Fan, Z.; Li, X.; Fu, L.; Wu, W. Nanotechnology-Assisted Sensors for the Detection of Carbon Monoxide: A Review. *Int. J. Electrochem. Sci.* **2023**, *18*, 100314. [\[CrossRef\]](#)
19. Qin, C.; Wei, Z.; Wang, B.; Wang, Y. Sn and Mn Co-Doping synergistically promotes the sensing properties of Co<sub>3</sub>O<sub>4</sub> sensor for high-sensitive CO detection. *Sens. Actuators B Chem.* **2023**, *390*, 133930. [\[CrossRef\]](#)
20. Pandit, N.A.; Ahmad, T. ZrO<sub>2</sub>/CeO<sub>2</sub>-Heterostructured Nanocomposites for Enhanced Carbon Monoxide Gas Sensing. *ACS Appl. Nano Mater.* **2023**, *6*, 7299–7309. [\[CrossRef\]](#)
21. Baier, D.; Priamushko, T.; Weinberger, C.; Kleitz, F.; Tiemann, M. Selective Discrimination between CO and H<sub>2</sub> with Copper-Ceria-Resistive Gas Sensors. *ACS Sens.* **2023**, *8*, 1616–1623. [\[CrossRef\]](#) [\[PubMed\]](#)
22. Agrawal, J.; Shukla, M.; Singh, V. Investigation of the Effect of ZnO Film Thickness over the Gas Sensor Developed for Sensing Carbon Monoxide. *Phys. Status Solidi (A) Appl. Mater. Sci.* **2023**, *220*, 2300047. [\[CrossRef\]](#)
23. Zhao, W.; Fam, D.W.H.; Yin, Z.; Sun, T.; Tan, H.T.; Liu, W.; Tok, A.I.Y.; Boey, Y.C.F.; Zhang, H.; Hng, H.H.; et al. A Carbon Monoxide Gas Sensor Using Oxygen Plasma Modified Carbon Nanotubes. *Nanotechnology* **2012**, *23*, 425502. [\[CrossRef\]](#) [\[PubMed\]](#)
24. Afrin, R.; Shah, N.A. Room Temperature Gas Sensors Based on Carboxyl and Thiol Functionalized Carbon Nanotubes Buckypapers. *Diam. Relat. Mater.* **2015**, *60*, 42–49. [\[CrossRef\]](#)
25. Panda, D.; Nandi, A.; Datta, S.K.; Saha, H.; Majumdar, S. Selective Detection of Carbon Monoxide (CO) Gas by Reduced Graphene Oxide (RGO) at Room Temperature. *RSC Adv.* **2016**, *6*, 47337–47348. [\[CrossRef\]](#)
26. Simões, A.N.; Lustosa, G.M.M.M.; de Souza Morita, E.; de Souza, A.N.; Torres, F.; Bizzo, W.A.; Mazon, T. Room-Temperature SnO<sub>2</sub>-Based Sensor with Pd-Nanoparticles for Real-Time Detection of CO Dissolved Gas in Transformer Oil. *Mater. Chem. Phys.* **2024**, *311*, 128576. [\[CrossRef\]](#)
27. Fort, A.; Landi, E.; Mugnaini, M.; Parri, L.; Pozzebon, A.; Vignoli, V. A LoRaWAN Carbon Monoxide Measurement System with Low-Power Sensor Triggering for the Monitoring of Domestic and Industrial Boilers. *IEEE Trans. Instrum. Meas.* **2021**, *70*, 5500609. [\[CrossRef\]](#)
28. Mahajan, S.; Jagtap, S. Metal-Oxide Semiconductors for Carbon Monoxide (CO) Gas Sensing: A Review. *Appl. Mater. Today* **2020**, *18*, 100483. [\[CrossRef\]](#)
29. Lawaniya, S.D.; Kumar, S.; Yu, Y.; Rubahn, H.G.; Mishra, Y.K.; Awasthi, K. Functional Nanomaterials in Flexible Gas Sensors: Recent Progress and Future Prospects. *Mater. Today Chem.* **2023**, *29*, 101428. [\[CrossRef\]](#)
30. Jiao, M.Z.; Chen, X.Y.; Hu, K.X.; Qian, D.Y.; Zhao, X.H.; Ding, E.J. Recent Developments of Nanomaterials-Based Conductive Type Methane Sensors. *Rare Met.* **2021**, *40*, 1515–1527. [\[CrossRef\]](#)
31. Yamazoe, N.; Shimano, K. New Perspectives of Gas Sensor Technology. *Sens. Actuators B Chem.* **2009**, *138*, 100–107. [\[CrossRef\]](#)
32. Blackman, C. Do We Need “Ionisorbed” Oxygen Species? (Or, “a Surface Conductivity Model of Gas Sensitivity in Metal Oxides Based on Variable Surface Oxygen Vacancy Concentration”). *ACS Sens.* **2021**, *6*, 3509–3516. [\[CrossRef\]](#) [\[PubMed\]](#)
33. Degler, D. Trends and Advances in the Characterization of Gas Sensing Materials Based on Semiconducting Oxides. *Sensors* **2018**, *18*, 3544. [\[CrossRef\]](#) [\[PubMed\]](#)
34. Chen, Y.; Meng, Q.; Zhang, L.; Han, C.; Gao, H.; Zhang, Y.; Yan, H. SnO<sub>2</sub>-Based Electron Transporting Layer Materials for Perovskite Solar: A Review of Recent Progress. *J. Energy Chem.* **2019**, *35*, 144–167. [\[CrossRef\]](#)
35. Zhang, Y.; Cui, S.; Chang, J.; Ocola, L.E.; Chen, J. Highly Sensitive Room Temperature Carbon Monoxide Detection Using SnO<sub>2</sub> Nanoparticle-Decorated Semiconducting Single-Walled Carbon Nanotubes. *Nanotechnology* **2013**, *24*, 025503. [\[CrossRef\]](#) [\[PubMed\]](#)
36. Bai, M.; Chen, M.; Li, X.; Wang, Q. One-Step CVD Growth of ZnO Nanorod/SnO<sub>2</sub> Film Heterojunction for NO<sub>2</sub> Gas Sensor. *Sens. Actuators B Chem.* **2022**, *373*, 132738. [\[CrossRef\]](#)

37. Yang, A.; Tao, X.; Wang, R.; Lee, S.; Surya, C. Room Temperature Gas Sensing Properties of SnO<sub>2</sub>/Multiwall-Carbon-Nanotube Composite Nanofibers. *Appl. Phys. Lett.* **2007**, *91*, 133110. [[CrossRef](#)]
38. Shojaee, M.; Nasresfahani, S.; Sheikhi, M.H. Hydrothermally Synthesized Pd-Loaded SnO<sub>2</sub>/Partially Reduced Graphene Oxide Nanocomposite for Effective Detection of Carbon Monoxide at Room Temperature. *Sens. Actuators B Chem.* **2018**, *254*, 457–467. [[CrossRef](#)]
39. Nguyen, V.D.; Duong, T.T.; Dang, T.T.; Chu, M.H.; Matteo, T.; Hugo, N.; Nguyen, D.H. Enhancement of NH<sub>3</sub> Gas Sensing with Ag-Pt Co-Catalyst on SnO<sub>2</sub> Nanofilm towards Medical Diagnosis. *Thin Solid Films* **2023**, *767*, 139682. [[CrossRef](#)]
40. Nguyen, V.D.; Nguyen, X.T.; Trinh, M.N.; Dang, T.T.; Chu, M.H.; Hugo, N.; Matteo, T.; Nguyen, V.H.; Nguyen, D.H. Design and Fabrication of Effective Gradient Temperature Sensor Array Based on Bilayer SnO<sub>2</sub>/Pt Gas Classification. *Sens. Actuators B Chem.* **2022**, *351*, 130979. [[CrossRef](#)]
41. Emanuel, P.N.; Hellen, C.T.F.; Gelmires, A.N.; Romualdo, R.M. A Review of Recent Developments in Tin Dioxide Nanostructured Materials for Gas Sensors. *Ceram. Int.* **2022**, *48*, 7405–7440. [[CrossRef](#)]
42. Manjula, P.; Arunkumar, S.; Manorama, S.V. Au/SnO<sub>2</sub> an Excellent Material for Room Temperature Carbon Monoxide Sensing. *Sens. Actuators B Chem.* **2011**, *152*, 168–175. [[CrossRef](#)]
43. Matsushima, S.; Teraoka, Y.; Norio, M.; Yamazoe, N. Electronic Interaction between Metal Additives and Tin Dioxide in Tin Dioxide-Based Gas Sensors. *Jpn. J. Appl. Phys.* **1988**, *27*, 1798–1802. [[CrossRef](#)]
44. Wang, K.; Zhao, T.; Lian, G.; Yu, Q.; Luan, C.; Wang, Q.; Cui, D. Room Temperature CO Sensor Fabricated from Pt-Loaded SnO<sub>2</sub> Porous Nanosolid. *Sens. Actuators B Chem.* **2013**, *184*, 33–39. [[CrossRef](#)]
45. Kang, K.-S.; Lee, S.P. CO Gas Sensors Operating at Room Temperature. *J. Mater. Sci.* **2003**, *38*, 4319–4323. [[CrossRef](#)]
46. Liu, H.; Chen, Y.; Dong, Z.; Wang, X.; Xu, J. The Preparation of CH<sub>3</sub>NH<sub>3</sub>SnI<sub>3</sub>/SnO<sub>2</sub>/Pd/Au Gas Sensor Material for Detecting CO and the Function of Each Component. *J. Mater. Sci. Mater. Electron.* **2022**, *33*, 7463–7476. [[CrossRef](#)]
47. Zhu, S.; Liu, Y.; Wu, G.; Fei, L.; Zhang, S.; Hu, Y.; Yan, Z.; Wang, Y.; Gu, H.; Chen, W. Mechanism Study on Extraordinary Room-Temperature CO Sensing Capabilities of Pd-SnO<sub>2</sub> Composite Nanoceramics. *Sens. Actuators B Chem.* **2019**, *285*, 49–55. [[CrossRef](#)]
48. Kishnani, V.; Verma, G.; Pippara, R.K.; Yadav, A.; Chauhan, P.S.; Gupta, A. Highly Sensitive, Ambient Temperature CO Sensor Using Tin Oxide Based Composites. *Sens. Actuators A Phys.* **2021**, *332*, 113111. [[CrossRef](#)]
49. Marikutsa, A.; Rumyantseva, M.; Gaskov, A. Specific Interaction of PdO<sub>x</sub>- and RuO<sub>y</sub>-Modified Tin Dioxide with CO and NH<sub>3</sub> Gases: Kelvin Probe and DRIFT Studies. *J. Phys. Chem. C* **2015**, *119*, 24342–24350. [[CrossRef](#)]
50. Li, L.; Wang, C.; Ying, Z.; Wu, W.; Hu, Y.; Yang, W.; Xuan, W.; Li, Y.; Wen, F. SnO<sub>2</sub>/Graphene Nanocomposite for Effective Detection of CO at Room Temperature. *Chem. Phys. Lett.* **2023**, *830*, 140803. [[CrossRef](#)]
51. Pineda-Reyes, A.M.; Herrera-Rivera, M.R.; Rojas-Chávez, H.; Cruz-Martínez, H.; Medina, D.I. Recent Advances in ZnO-Based Carbon Monoxide Sensors: Role of Doping. *Sensors* **2021**, *21*, 4425. [[CrossRef](#)]
52. Heo, Y.W.; Norton, D.P.; Tien, L.C.; Kwon, Y.; Kang, B.S.; Ren, F.; Pearton, S.J.; Laroche, J.R. ZnO Nanowire Growth and Devices. *Mater. Sci. Eng. R Rep.* **2004**, *47*, 1–47. [[CrossRef](#)]
53. Schmidt-Mende, L.; Macmanus-Driscoll, J.L. ZnO-Nanostructures, Defects, and Devices. *Mater. Today* **2007**, *10*, 40–48. [[CrossRef](#)]
54. Zhu, L.; Zeng, W. Room-Temperature Gas Sensing of ZnO-Based Gas Sensor: A Review. *Sens. Actuators A Phys.* **2017**, *267*, 242–261. [[CrossRef](#)]
55. Huang, M.H.; Wu, Y.; Feick, H.; Tran, N.; Weber, E.; Yang, P. Catalytic Growth of Zinc Oxide Nanowires by Vapor Transport. *Adv. Mater.* **2001**, *13*, 113–116. [[CrossRef](#)]
56. Xu, S.; Wang, Z.L. One-Dimensional ZnO Nanostructures: Solution Growth and Functional Properties. *Nano Res.* **2011**, *4*, 1013–1098. [[CrossRef](#)]
57. Wang, L.; Kang, Y.; Liu, X.; Zhang, S.; Huang, W.; Wang, S. ZnO Nanorod Gas Sensor for Ethanol Detection. *Sens. Actuators B Chem.* **2012**, *162*, 237–243. [[CrossRef](#)]
58. Wang, J.X.; Sun, X.W.; Yang, Y.; Huang, H.; Lee, Y.C.; Tan, O.K.; Vayssieres, L. Hydrothermally Grown Oriented ZnO Nanorod Arrays for Gas Sensing Applications. *Nanotechnology* **2006**, *17*, 4995–4998. [[CrossRef](#)]
59. Yuan, Z.; Jiaqiang, X.; Qun, X.; Hui, L.; Qingyi, P.; Pengcheng, X. Brush-like Hierarchical ZnO Nanostructures: Synthesis, Photoluminescence and Gas Sensor Properties. *J. Phys. Chem. C* **2009**, *113*, 3430–3435. [[CrossRef](#)]
60. Alenezi, M.R.; Henley, S.J.; Emerson, N.G.; Silva, S.R.P. From 1D and 2D ZnO Nanostructures to 3D Hierarchical Structures with Enhanced Gas Sensing Properties. *Nanoscale* **2014**, *6*, 235–247. [[CrossRef](#)]
61. Pan, X.; Zhao, X. Ultra-High Sensitivity Zinc Oxide Nanocombs for on-Chip Room Temperature Carbon Monoxide Sensing. *Sensors* **2015**, *15*, 8919–8930. [[CrossRef](#)] [[PubMed](#)]
62. Jamshidi Bandari, A.; Nasirian, S. Carbon Monoxide Gas Sensing Features of Zinc Oxide Nanoneedles: Practical Selectivity and Long-Term Stability. *J. Mater. Sci. Mater. Electron.* **2019**, *30*, 10073–10081. [[CrossRef](#)]
63. Joshi, R.K.; Hu, Q.; Alvi, F.; Joshi, N.; Kumar, A. Au Decorated Zinc Oxide Nanowires for CO Sensing. *J. Phys. Chem. C* **2009**, *113*, 16199–16202. [[CrossRef](#)]
64. Arunkumar, S.; Hou, T.; Kim, Y.B.; Choi, B.; Park, S.H.; Jung, S.; Lee, D.W. Au Decorated ZnO Hierarchical Architectures: Facile Synthesis, Tunable Morphology and Enhanced CO Detection at Room Temperature. *Sens. Actuators B Chem.* **2017**, *243*, 990–1001. [[CrossRef](#)]

65. Schipani, F.; Villegas, E.A.; Ramajo, L.A.; Parra, R. Zinc Oxide Thin Films for a Room Temperature Dual Carbon Dioxide and Carbon Monoxide Sensor. *J. Mater. Sci. Mater. Electron.* **2023**, *34*, 1092. [[CrossRef](#)]
66. Wang, D.; Zhang, D.; Pan, Q.; Wang, T.; Chen, F. Gas Sensing Performance of Carbon Monoxide Sensor Based on Rod-Shaped Tin Diselenide/MOFs Derived Zinc Oxide Polyhedron at Room Temperature. *Sens. Actuators B Chem.* **2022**, *371*, 132481. [[CrossRef](#)]
67. Yu, M.R.; Wu, R.J.; Chavali, M. Effect of "Pt" Loading in ZnO-CuO Hetero-Junction Material Sensing Carbon Monoxide at Room Temperature. *Sens. Actuators B Chem.* **2011**, *153*, 321–328. [[CrossRef](#)]
68. Cozzoli, P.D.; Kornowski, A.; Weller, H. Low-Temperature Synthesis of Soluble and Processable Organic-Capped Anatase TiO<sub>2</sub> Nanorods. *J. Am. Chem. Soc.* **2003**, *125*, 14539–14548. [[CrossRef](#)]
69. Galstyan, V.; Comini, E.; Faglia, G.; Sberveglieri, G. TiO<sub>2</sub> Nanotubes: Recent Advances in Synthesis and Gas Sensing Properties. *Sensors* **2013**, *13*, 14813–14838. [[CrossRef](#)]
70. Galstyan, V. Porous TiO<sub>2</sub>-Based Gas Sensors for Cyber Chemical Systems to Provide Security and Medical Diagnosis. *Sensors* **2017**, *17*, 2947. [[CrossRef](#)]
71. Kumarage, G.W.C.; Hakkoum, H.; Comini, E. Recent Advancements in TiO<sub>2</sub> Nanostructures: Sustainable Synthesis and Gas Sensing. *Nanomaterials* **2023**, *13*, 1424. [[CrossRef](#)] [[PubMed](#)]
72. Wu, R.J.; Chang, W.C.; Tsai, K.M.; Wu, J.G. The Novel CO Sensing Material CoOOH-WO<sub>3</sub> with Au and SWCNT Performance Enhancement. *Sens. Actuators B Chem.* **2009**, *138*, 35–41. [[CrossRef](#)]
73. Bittencourt, C.; Felten, A.; Espinosa, E.H.; Ionescu, R.; Llobet, E.; Correig, X.; Pireaux, J.J. WO<sub>3</sub> Films Modified with Functionalised Multi-Wall Carbon Nanotubes: Morphological, Compositional and Gas Response Studies. *Sens. Actuators B Chem.* **2006**, *115*, 33–41. [[CrossRef](#)]
74. Al-Kuhaili, M.F.; Durrani, S.M.A.; Bakhtiari, I.A. Carbon Monoxide Gas-Sensing Properties of CeO<sub>2</sub>-WO<sub>3</sub> Thin Films. *Mater. Sci. Technol.* **2010**, *26*, 726–731. [[CrossRef](#)]
75. Estanto; Septiani, N.L.W.; Iqbal, M.; Suyatman; Nuruddin, A.; Yulianto, B. Nanocomposite of Graphene and WO<sub>3</sub> Nanowires for Carbon Monoxide Sensors. *Nanocomposites* **2021**, *7*, 225–236. [[CrossRef](#)]
76. Chen, K.W.; Liu, J.P.; Hsu, Y.S.; Liu, C.H.; Pai, Y.H.; Chen, C.H. Controlled Synthesis of Pt and Co<sub>3</sub>O<sub>4</sub> Dual-Functionalized In<sub>2</sub>O<sub>3</sub> Nanoassemblies for Room Temperature Detection of Carbon Monoxide. *New J. Chem.* **2018**, *42*, 16478–16482. [[CrossRef](#)]
77. Geng, B.; Zhan, F.; Jiang, H.; Xing, Z.; Fang, C. Facile Production of Self-Assembly Hierarchical Dumbbell-like CoOOH Nanostructures and Their Room-Temperature CO-Gas-Sensing Properties. *Cryst. Growth Des.* **2008**, *8*, 3497–3500. [[CrossRef](#)]
78. Kumar, M.; Kumar, D.; Gupta, A.K. Fe-Doped TiO<sub>2</sub> Thin Films for CO Gas Sensing. *J. Electron. Mater.* **2015**, *44*, 152–157. [[CrossRef](#)]
79. Ye, X.L.; Lin, S.J.; Zhang, J.W.; Jiang, H.J.; Cao, L.A.; Wen, Y.Y.; Yao, M.S.; Li, W.H.; Wang, G.E.; Xu, G. Boosting Room Temperature Sensing Performances by Atomically Dispersed Pd Stabilized via Surface Coordination. *ACS Sens.* **2021**, *6*, 1103–1110. [[CrossRef](#)]
80. Su, J.; Zou, X.X.; Zou, Y.C.; Li, G.D.; Wang, P.P.; Chen, J.S. Porous Titania with Heavily Self-Doped Ti<sup>3+</sup> for Specific Sensing of CO at Room Temperature. *Inorg. Chem.* **2013**, *52*, 5924–5930. [[CrossRef](#)]
81. Kumar, M.; Gupta, A.K.; Kumar, D. Mg-Doped TiO<sub>2</sub> Thin Films Deposited by Low Cost Technique for CO Gas Monitoring. *Ceram. Int.* **2016**, *42*, 405–410. [[CrossRef](#)]
82. Wei, W.; Zhang, H.; Tao, T.; Xia, X.; Bao, Y.; Lourenço, M.; Homewood, K.; Huang, Z.; Gao, Y. A CuO/TiO<sub>2</sub> Heterojunction Based CO Sensor with High Response and Selectivity. *Energy Environ. Mater.* **2023**, *6*, e12570. [[CrossRef](#)]
83. Wu, Y.; Li, J.; Lv, M.; Zhang, X.; Gao, R.; Guo, C.; Cheng, X.; Zhou, X.; Xu, Y.; Gao, S.; et al. Selective Detection of Trace Carbon Monoxide at Room Temperature Based on CuO Nanosheets Exposed to (111) Crystal Facets. *J. Hazard. Mater.* **2023**, *442*, 130041. [[CrossRef](#)] [[PubMed](#)]
84. Adeyemo, A.; Hunter, G.; Dutta, P.K. Interaction of CO with Hydrous Ruthenium Oxide and Development of a Chemoresistive Ambient CO Sensor. *Sens. Actuators B Chem.* **2011**, *152*, 307–315. [[CrossRef](#)]
85. Li, H.; Wu, J.; Yin, Z.; Zhang, H. Preparation and Applications of Mechanically Exfoliated Single-Layer and Multilayer MoS<sub>2</sub> and WSe<sub>2</sub> Nanosheets. *Acc. Chem. Res.* **2014**, *47*, 1067–1075. [[CrossRef](#)] [[PubMed](#)]
86. Perkins, F.K.; Friedman, A.L.; Cobas, E.; Campbell, P.M.; Jernigan, G.G.; Jonker, B.T. Chemical Vapor Sensing with Monolayer MoS<sub>2</sub>. *Nano Lett.* **2013**, *13*, 668–673. [[CrossRef](#)] [[PubMed](#)]
87. Sadaf, S.; Zhang, H.; Akhtar, A. MoS<sub>2</sub>-NiO Nanocomposite for H<sub>2</sub>S Sensing at Room Temperature. *RSC Adv.* **2023**, *13*, 28564–28575. [[CrossRef](#)] [[PubMed](#)]
88. Kumar, A.; Sanger, A.; Kang, S.B.; Chandra, R. Interface Engineering-Driven Room-Temperature Ultralow Gas Sensors with Elucidating Sensing Performance of Heterostructure Transition Metal Dichalcogenide Thin Films. *ACS Sens.* **2023**, *8*, 3824–3835. [[CrossRef](#)] [[PubMed](#)]
89. Piosik, E.; Szary, M.J. Development of MoS<sub>2</sub> Doping Strategy for Enhanced SO<sub>2</sub> Detection at Room Temperature. *Appl. Surf. Sci.* **2023**, *638*, 158013. [[CrossRef](#)]
90. Choi, W.; Choudhary, N.; Han, G.H.; Park, J.; Akinwande, D.; Lee, Y.H. Recent Development of Two-Dimensional Transition Metal Dichalcogenides and Their Applications. *Mater. Today* **2017**, *20*, 116–130. [[CrossRef](#)]
91. Li, H.; Yin, Z.; He, Q.; Li, H.; Huang, X.; Lu, G.; Fam, D.W.H.; Tok, A.I.Y.; Zhang, Q.; Zhang, H. Fabrication of Single- and Multilayer MoS<sub>2</sub> Film-Based Field-Effect Transistors for Sensing NO at Room Temperature. *Small* **2012**, *8*, 63–67. [[CrossRef](#)] [[PubMed](#)]

92. Zhang, D.; Sun, Y.; Jiang, C.; Yao, Y.; Dongyue, W.; Zhang, Y. Room-Temperature Highly Sensitive CO Gas Sensor Based on Ag-Loaded Zinc Oxide/Molybdenum Disulfide Ternary Nanocomposite and Its Sensing Properties. *Sens. Actuators B Chem.* **2017**, *253*, 1120–1128. [[CrossRef](#)]
93. Zhang, D.; Wu, J.; Cao, Y. Cobalt-Doped Indium Oxide/Molybdenum Disulfide Ternary Nanocomposite toward Carbon Monoxide Gas Sensing. *J. Alloys Compd.* **2019**, *777*, 443–453. [[CrossRef](#)]
94. Li, Y.; Song, X.; Li, L.; Wu, W.; Tao, K.; Ying, Z.; Hu, Y.; Zhou, Y.; Zhang, R.; Wang, G.; et al. Low Concentration CO Gas Sensor Constructed from MoS<sub>2</sub> Nanosheets Dispersed SnO<sub>2</sub> Nanoparticles at Room Temperature under UV Light. *Ceram. Int.* **2023**, *49*, 10249–10254. [[CrossRef](#)]
95. Yang, Z.; Zhang, D.; Wang, D. Carbon Monoxide Gas Sensing Properties of Metal–Organic Frameworks-Derived Tin Dioxide Nanoparticles/Molybdenum Diselenide Nanoflowers. *Sens. Actuators B Chem.* **2020**, *304*, 127369. [[CrossRef](#)]
96. Staerz, A.; Weimar, U.; Barsan, N. Current State of Knowledge on the Metal Oxide Based Gas Sensing Mechanism. *Sens. Actuators B Chem.* **2022**, *358*, 131531. [[CrossRef](#)]
97. Degler, D.; Weimar, U.; Barsan, N. Current Understanding of the Fundamental Mechanisms of Doped and Loaded Semiconducting Metal-Oxide-Based Gas Sensing Materials. *ACS Sens.* **2019**, *4*, 2228–2249. [[CrossRef](#)] [[PubMed](#)]
98. Boehme, I.; Weimar, U.; Barsan, N. Unraveling the Surface Chemistry of CO Sensing with In<sub>2</sub>O<sub>3</sub> Based Gas Sensors. *Sens. Actuators B Chem.* **2021**, *326*, 129004. [[CrossRef](#)]
99. Fu, H.; Hou, C.; Gu, F.; Han, D.; Wang, Z. Facile Preparation of Rod-like Au/In<sub>2</sub>O<sub>3</sub> Nanocomposites Exhibiting High Response to CO at Room Temperature. *Sens. Actuators B Chem.* **2017**, *243*, 516–524. [[CrossRef](#)]

**Disclaimer/Publisher’s Note:** The statements, opinions and data contained in all publications are solely those of the individual author(s) and contributor(s) and not of MDPI and/or the editor(s). MDPI and/or the editor(s) disclaim responsibility for any injury to people or property resulting from any ideas, methods, instructions or products referred to in the content.